

# Pseudo-kinematic trajectory control of tracked vehicles

Michele Focchi<sup>1,3</sup>, Daniele Fontanelli<sup>2</sup>, Luigi Palopoli<sup>1</sup>

**Abstract**—Tracked vehicles are used in complex scenarios, where motion planning and navigation can be very complex. They have complex dynamics, with many parameters that are difficult to identify and that change significantly based on the operating conditions. We propose a simple pseudo-kinematic model, where the intricate dynamic effects underlying the vehicle’s motion are captured in a small set of velocity-dependent parameters. This choice enables the development of a Lyapunov-based trajectory controller with guaranteed performance and small computation time. We demonstrate the correctness of our approach with both simulation and experimental data.

## I. INTRODUCTION

Tracked mobile robots have a recognised resistance to slippage effects due to the large contact area between the tracks and the ground. This makes them a perfect fit for a large family of robot-assisted agricultural applications such as weed control, seeding, fertilisation, pest management, and crop harvesting. This flexibility comes with a price: the complexity of vehicle-ground interaction makes the system dynamics very complex, the parameters difficult to estimate and the system difficult to control.

Most of the difficulty lies in the so-called skid steering mechanism: due to the lateral rigidity of the tracks when a tracked vehicle follows a curved path, the entire track assembly must rotate at the same angular velocity as the vehicle. In other words, since the vehicle cannot rely on the pure rolling assumption of differential drive vehicles or on a separate driving mechanism a-la Ackermann, it is forced to skid its tracks on the ground when it turns. The motion of skid-steering vehicles is determined by the two longitudinal track forces and by the lateral friction force. Therefore, these vehicles control their heading exactly as differential-drive vehicles do, i.e., by varying the relative speed of the left and the right tracks. However, the lateral friction force depends on vehicle’s linear and angular velocities, which generates challenging and time varying non-holonomic constraints [1].

The angular velocities of the two track sprockets wheels serve as the system control inputs, while the vehicle’s motion is governed by both soil mechanics and vehicle dynamics.

**Related Work.** The soil mechanics is often characterised by empirical shear stress-slippage relationships, derived from a massive amount of experimental data [2], [3]. Because of the difficulties in the derivation of a theoretical model of the soil-track interaction, a simplified analytical soil model is usually



Fig. 1. Picture of the Maxxi tracked vehicle.

derived under the assumption of homogeneous soil and a uniformly distributed load along the tracks. These interaction forces reveals themselves as motion and slippages. Albeit the traction and lateral force can be used in the integration of dynamic models [4], track slip can be also related to purely *kinematic* effects by comparing the odometry-based track speed to the velocity of the vehicle.

In this direction, [5], [6] proposed an Extended Kalman Filter, while [7] proposed a Least Squares approach, to identify in real-time the soil-track slip parameters. Moosavian et al. [8], proposed to use an exponential to approximate the *longitudinal* slip as a function of the turning radius, an approximation that proved effective at low speeds. Piccinini et al. [9] explored the prediction of lateral slippage for wheeled vehicles using neural networks for motion planning. In the papers mentioned above, the longitudinal slip estimation is compensated through a feed-forward controller using a kinematic model.

Control solutions based on purely *kinematic* model are customary in the literature on non-holonomic vehicle control. Differential-drive vehicles are often modelled through a non-linear kinematic model. Trajectory control can be obtained using Lyapunov-based control strategies [10] or feedback linearisation [11]. Contrary to differential-drive robots, the vast majority of control solution for tracked vehicles are based on *dynamic* models [4], [12], [13], [14], because for these vehicles it is not possible to have a clean separation between kinematics and dynamics.

Zou et al. [12] employed non-linear feedback to convert the dynamic control challenge into a kinematic one. However, this type of approach relies on an exact knowledge of the model parameters to implement feedback linearisation, and under these conditions the robustness is far from obvious. Additionally, only simulation results were reported. More recently, Sabiha et al. [14] combined back-stepping with sliding mode control to design a trajectory tracking controller that accounts for track slippage. However, since their robot is operated at very low speeds, slippage effects are minor and the advantage of their strategy is far from apparent. The

<sup>1</sup> The authors are with the Dipartimento di Ingegneria and Scienza dell’Informazione (DISI), University of Trento, name.surname@unitn.it

<sup>2</sup> The authors is with the Dipartimento di Ingegneria Industriale (DII), University of Trento, daniele.fontanelli@unitn.it

complexity of modelling the interaction between track and terrain, has pushed toward the adoption of *pseudo-kinematic* models, where the dynamic effects are embedded into a small set of parameters [15], but the way these models can be used for control has not been explored to a sufficient degree.

**Paper Contribution and Summary.** The approach proposed in this paper is based on a *pseudo-kinematic* model of a tracked vehicle that includes lateral slippage, inspired by [12]. The control law we propose also features a feed-forward compensation for the longitudinal slippage, which we discovered has a more complex relationship on the turning radius than frequently assumed [8] (our data reveal also a dependency from the absolute value of the longitudinal speed).

The pseudo-kinematic model reveals an important dependence between lateral slippage and robot velocity. This relation leads to a peculiar under-steering behaviour that becomes important at relatively high speeds, and that our feedback law takes into account. An important problem of standard models [8] is a singularity due to an asymptote in the *longitudinal* slippage when the turning radius approaches the half of the vehicle width. We avoid this singularity by choosing an isomorphic parametrisation that relates the *longitudinal* slippage to the sprocket wheel speeds. Thanks to our controller, the vehicle's behaviour approximates that of a unicycle simplifying motion planning, for which we can use standard Dubins manoeuvres [16]. To summarise, the main contributions of this paper are twofold: i) The design of a slippage-aware, Lyapunov-based tracking controller for a pseudo-kinematic model of a tracked vehicle (Section IV). ii) A novel approach for identifying and predicting the longitudinal slippage using wheel speed inputs, based on machine learning techniques, validated with real experimental data from a Maxxi robot (Fig. 1 and Section III). The controller's effectiveness and the resulting improvements in tracking accuracy are evaluated through simulations, utilizing a dynamic model that incorporates realistic terrain interactions, modeled using a distributed parameter approach (Section II-A).

## II. MODELING

In this section, we present two models of a tracked vehicle: i) a dynamic model, accounting for realistic terrain interactions, that will be used in the simulation and ii) a pseudo-kinematic model used for the synthesis of the control law. The underlying assumption for the derivation of both models is that the terrain is flat.

### A. Dynamic model for a tracked vehicle

On firm ground, with negligible adhesion, the relationship shear-stress shear-displacement are expressed by [3]:

$$\tau = \sigma\mu \left(1 - e^{-\|j\|/K}\right) \quad (1)$$

where  $\mu$  is the friction coefficient between the track and the ground,  $\sigma$  is the normal pressure, and  $j = [j_x, j_y] \in \mathbb{R}^2$  is the shear displacement of a certain contact location. Forces and torques exchanged with the ground are obtained

by integration of the infinitesimals exerted on small contact areas on the track, i.e.

$$dF_{\text{long}} = -\tau(x_p, y_p, v_x, \omega, \omega_{L/R}) \cos \delta dA, \quad (2)$$

$$dF_{\text{lat}} = -\tau(x_p, y_p, v_x, \omega, \omega_{L/R}) \sin \delta dA, \quad (3)$$

$$dM_{\text{long}} = -y_p dF_{\text{long}}, \quad dM_{\text{lat}} = x_p dF_{\text{lat}}, \quad (4)$$

where  $\omega_{L/R}$  are the wheel sprocket speed of the left/right track,  $(x_p, y_p)$  is the location of the contact patch in the body frame,  $v_x$  is the vehicle longitudinal speed,  $\omega$  its angular velocity of the robot w.r.t. the vertical axis (see Fig. 2) and  $\delta$  is the direction of the patch's shear velocity (refer to [3] for details on the computation of  $\delta$ ). Since the integration cannot be solved analytically, we divide each tracks into  $n$  sub-areas. Then, for a tracked vehicle of mass  $m$  with a

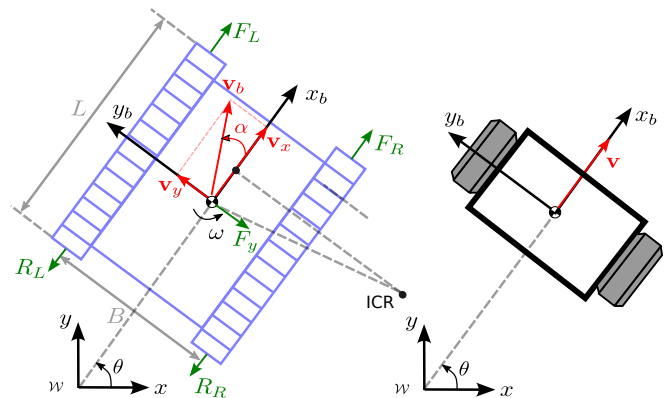


Fig. 2. Top view of (left) a differentially steered tracked mobile robot and (right) of its unicycle approximation. The standard definitions for frames and variables are also provided.

moment of inertia  $I_{zz}$  about a vertical axis passing through the center of mass, the equations of motion can be written (in the body frame) as:

$$m(\dot{v}_x - \omega v_y) = \underbrace{F_{\text{long},L} + F_{\text{long},R}}_{F_t} - \underbrace{(R_L + R_R)}_{R_t}, \quad (5)$$

$$m(\dot{v}_y + \omega v_x) = \underbrace{F_{\text{lat},L} + F_{\text{lat},R}}_{F_y},$$

$$I_{zz}\dot{\omega} = \underbrace{M_{\text{long},L} + M_{\text{long},R}}_{M_t} + \underbrace{M_{\text{lat},L} + M_{\text{lat},R}}_{M_r} - \frac{B}{2}(R_R + R_L),$$

where  $\mathbf{v} = [v_x, v_y] \in \mathbb{R}^2$  is the velocity of the vehicle in the base frame. Moreover,  $F_t$  is the total traction force,  $R_t$  is the total *longitudinal* resistive force to the track movement (i.e. due to friction),  $F_y$  the total *lateral* resistive force,  $M_t$  is the turning moment,  $M_r$  the turning resistance moment and  $B$  is the distance between the two interlines of the tracks.

We parametrize the three-dimensional configuration space and its tangent mapping as:

$$\eta = \begin{bmatrix} x \\ y \end{bmatrix} \in \mathbb{R}^2 \times S, \quad \dot{\eta} = \begin{bmatrix} \dot{x} \\ \dot{y} \\ \dot{\theta} \end{bmatrix} = \begin{bmatrix} \mathbf{R}(\theta) & \mathbf{0} \\ \mathbf{0}^T & 1 \end{bmatrix} \begin{bmatrix} v_x \\ v_y \\ \omega \end{bmatrix}, \quad (6)$$

TABLE I  
SIMULATION PARAMETERS

| Name                               | Symbol   | Value  |
|------------------------------------|----------|--------|
| Inertia moment [kgm <sup>2</sup> ] | $I_{zz}$ | 4.5    |
| Robot mass [kg]                    | $m$      | 62     |
| Track width [m]                    | $B$      | 0.606  |
| Sprocket radius                    | $r$      | 0.0856 |

where  $\theta$  is the heading angle of the vehicle (about the axis  $z$ , which is pointing up), and  $x$  and  $y$  its Cartesian position in absolute coordinates. Throughout this work, the symbol  $\mathbb{R}^n$  is the Euclidean space of dimension  $n$ ,  $S$  the set of Euler angles defined on the interval  $[-\pi \ \pi]$ ,  $SO(3)$  is the Special Orthogonal Group of order 3, while vectors are reported using bold symbols. The parameters for this model are listed in Table I.

### B. Pseudo-Kinematic model: Tracked robot model

Before presenting the pseudo-kinematic model we first introduce the *unicycle* model which is instrumental for the next derivation. A differentially driven mobile robot can be modeled as shown in Fig. 2-(right), where the speeds of the two wheels can be independently controlled to provide a desired longitudinal speed  $v = v_x$  (i.e. along the body  $x_b$  axis) and a yaw rate  $\omega$ . Let the state of the system be its pose, if the pure rolling condition holds (i.e., the sway speed  $v_y$  is identically zero), the kinematic equations are notoriously given by:

$$\begin{aligned}\dot{x} &= v \cos(\theta), \\ \dot{y} &= v \sin(\theta), \\ \dot{\theta} &= \omega,\end{aligned}\quad (7)$$

where  $x$  and  $y$  are the Cartesian coordinates expressed in the world frame,  $\theta$  is the orientation with respect to the  $x$ -axis. It is possible to relate the inputs  $v, \omega$  to the left/right sprocket wheel velocities of the tracks  $\omega_L$  and  $\omega_R$  by an affine mapping:

$$\begin{bmatrix} v \\ \omega \end{bmatrix} = \begin{bmatrix} \frac{r}{2} & \frac{r}{2} \\ -\frac{r}{B} & \frac{r}{B} \end{bmatrix} \begin{bmatrix} \omega_L \\ \omega_R \end{bmatrix}\quad (8)$$

In the rest of this paper, we will use the  $d$  subscript (e.g.,  $(x_d, y_d, \theta_d)$  or  $(v_d, \omega_d)$ ) to denote desired quantities.

On the other hand, regarding a tracked vehicle, in the adopted kinematic model [12] the terrain-interactions are lumped into three parameters, namely: the *lateral* slippage angle  $\alpha$  and the left and right track *longitudinal* slippages  $\beta_L$  and  $\beta_R$ , respectively. The kinematics equations are given by [12], [14], i.e.

$$\begin{aligned}\dot{x} &= \frac{v}{\cos(\alpha)} \cos(\theta + \alpha), \\ \dot{y} &= \frac{v}{\cos(\alpha)} \sin(\theta + \alpha), \\ \dot{\theta} &= \omega,\end{aligned}\quad (9)$$

where the lateral slip angle  $\alpha$  represents the deviation of the velocity vector w.r.t. the  $x_b$  axis due to the lateral slippage (hence, along the  $y_b$  axis, as in Fig. 2-(left)), which derives from the skid steering behavior, coming from the action of

the lateral force  $F_y$  presented in the previous section.  $\alpha$  can be computed from the actual velocity measurements by means of

$$\alpha = \tan^{-1} \left( \frac{v_y}{v_x} \right).\quad (10)$$

Using the functional dependency of  $\alpha$  from the turning radius  $R = \frac{v}{\omega}$  (see [17], [18]), we propose the following exponential parametrization

$$\alpha = f(r) = \begin{cases} -c_1 e^{-c_2 R}, & \text{if } R \geq 0, \\ c_1 e^{c_2 R}, & \text{if } R < 0, \end{cases}\quad (11)$$

where  $c_1 > 0$  and  $c_2 > 0$  are two constants that embed the terrain specificity and that are identified based on the type of track and terrain. It has to be noted that the slip angle increases with the path curvature (i.e., decreases with the turning radius), and it is positive for a clockwise turn, negative for a counter clockwise turn, and zero for straight line motions. The value of the slip angle is tightly interconnected to the (forward) shift of the Instantaneous Center of Rotation (ICR) during a turning maneuver [1]. On the other hand, the *longitudinal* slippage (i.e., along  $x_b$  axis, as in Fig. 2-(left)) *directly* affects the wheel speed by modifying the inputs (8) to (9). From kinematics the track velocities can be related to  $v$  and  $\omega$  by

$$v_L^t = v - \omega \frac{B}{2}, \quad v_R^t = v + \omega \frac{B}{2},\quad (12)$$

we have immediately that

$$\beta_L = v_L^t - \omega_L r, \quad \beta_R = v_R^t - \omega_R r.\quad (13)$$

where the left/right sprocket wheel velocities  $\omega_L$  and  $\omega_R$  are obtained by the encoder readings. The longitudinal slip is defined to be positive when the tractive effort produced assists the longitudinal motion (i.e. outer turning wheel) and negative otherwise (e.g. inner turning wheel). Note that while  $\beta_L$  and  $\beta_R$  affect directly the inputs and can be compensated in a feed-forward fashion in (8), in the case of  $\alpha$  there is an indirect dependency on the inputs through the dynamics. This motivates our choice of accounting for this effect directly in the controller design of Section IV.

### III. SLIPPAGE IDENTIFICATION

In this section, the experimental identification of the lateral and the longitudinal slippage are presented separately due to their different nature.

a) *Lateral slippage*: In this case, we employ the exponential function (11) to fit the data, considering the curvature radius as input. For this identification test, we commanded the robot's sprocket wheel speeds (in open loop) to generate a spiral-like trajectory of decreasing radius of curvature starting from  $R = 0.6$  m to  $R = 0.1$  m with decrements of 0.05 m. The tests have been performed at a constant longitudinal speed of  $v = 0.2$  m/s in simulation  $v = 0.1$  m/s in experiments. In this case we tested on a high friction (i.e. rubber floor) and a low friction terrain. The lower speed for the experiments is dictated by the actuator limits of

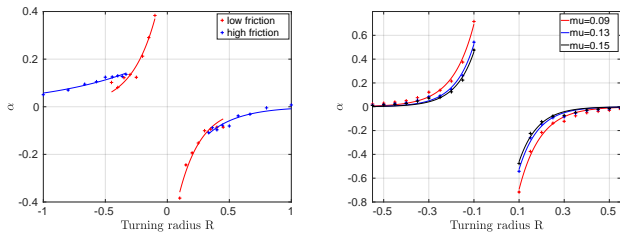


Fig. 3. Fitting of slide slippage parameter  $\alpha$  as function of the turning radius. (left) Experiments at  $v = 0.1$  m/s for the different terrains. (right) Simulation at  $v = 0.2$  m/s for different values of the friction coefficient  $\mu$ .

TABLE II  
IDENTIFICATION OF SIDE SLIP PARAMETERS

| Sim                        |        |       | Real     |       |       |
|----------------------------|--------|-------|----------|-------|-------|
| friction coefficient $\mu$ | $c_1$  | $c_2$ | Terrain  | $c_1$ | $c_2$ |
| 0.091                      | -1.22  | -8.18 | low fr.  | -0.63 | -5.56 |
| 0.133                      | -0.88  | -8.41 | high fr. | -0.22 | -1.34 |
| 0.156                      | -0.765 | -8.48 | x        | x     | x     |

the available robot. In the high friction tests, larger turning radii were considered because friction turned out to be very with high path curvatures. Moreover, wheel speeds were set constant (for a specific turning radius), during an interval of 8 s to let the system achieve a steady state velocity. Finally, the average of  $\alpha$  angle is computed for each turning radius.

Figure 3-(left) show experimental results with the Maxxi robot [19] for the high and low friction experiments. In simulation, we repeated the identification for different values of the friction coefficient  $\mu \in \{0.091, 0.133, 0.156\}$ , reported in Figure 3-(right) using the distributed parameter model (5). Overall, Figure 3 shows the exponential dependency of  $\alpha$  from the turning radius and demonstrate a good match between simulation and real experiments. The results of the identification are also quantitatively reported in Table II.

*b) Longitudinal Slippage:* Regarding the longitudinal slippage, we found a dependency not only on turning radius (as claimed in [8]) but also on the vehicle absolute velocity in the range of speeds of our interest. Therefore, rather than using a 1D kernel function (e.g. an exponential) we propose to design a multiple-input regressor based on decision trees for the values of  $\beta_L$  and  $\beta_R$ . The inputs of the regressor are the wheel sprocket speeds  $\omega_L$  and  $\omega_R$  instead of the turning radius, thus solving the singularity issue popping out when the velocity of the inner wheel becomes zero and the turning radius  $R$  is equal to half the distance from the two wheels [8]. For the identification of  $\beta_L$  and  $\beta_R$ , we uniformly sample wheel speeds in the set  $\{-7, 7\}$  rad/s with increments 0.05 rad/s. A comparison of the regressor prediction with the ground-truth values (sampled from a test set different from the training one) is given in Fig. 4 for left and right track, respectively, and for both simulation and experiments. Here the good fit of the regressor prediction with the acquired data, both for the simulation ( $R^2$  for  $\beta_L$ : 0.998,  $\beta_R$ : 0.998) and the experiments ( $R^2$  for  $\beta_L$ : 0.92,  $\beta_R$ : 0.86) is shown, thus proving the same trend for the simulation and the real experiments.

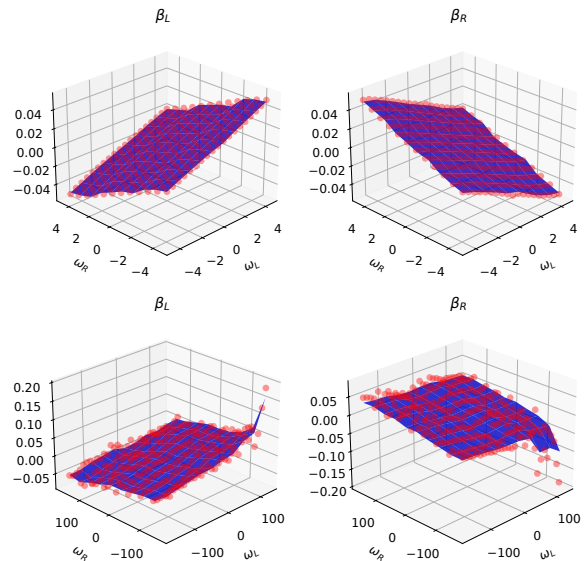


Fig. 4. Fitting of the longitudinal slippage parameters  $\beta_L$  (left) and  $\beta_R$  (right) as a function of the sprocket wheel speeds  $\omega_L$  and  $\omega_R$ . The row above shows the simulation results, while the bottom row plots the experimental data. The blue surface is the fit of the regressor predictions, while the red dots are the acquired data.

#### IV. CONTROL LAW DESIGN

The Lyapunov-based control law design is presented in this section. We briefly subsumes a trajectory following control law for the *unicycle*-like model (7), which is then adapted to the case of the tracked robot model (9).

*a) Useful Definitions:* In the context of trajectory tracking, we denote with  $(x_d, y_d, \theta_d)$  the desired quantities, which act as reference for the system state  $(x, y, \theta)$ . It is therefore useful to define the error vector

$$\mathbf{e} = \begin{bmatrix} e_x \\ e_y \\ e_\theta \end{bmatrix} = \begin{bmatrix} x - x_d \\ y - y_d \\ \theta - \theta_d \end{bmatrix}. \quad (14)$$

In the rest of this section, we use the following definitions:

$$e_{xy} = \left\| \begin{bmatrix} e_x \\ e_y \end{bmatrix} \right\| = \sqrt{e_x^2 + e_y^2}, \quad \psi = \text{atan2}(e_y, e_x), \quad (15)$$

$$e_x = e_{xy} \cos(\psi), \quad e_y = e_{xy} \sin(\psi).$$

##### A. Lyapunov-Based Control for a unicycle

The following control law for a unicycle-like vehicle will be used as a reference for the tracked vehicle control. Given the dynamics (7), we aim to develop a control law that ensures the convergence of the actual trajectory to the desired one. To this end, consider the Lyapunov function

$$V = \frac{1}{2} (e_x^2 + e_y^2) + (1 - \cos(e_\theta)), \quad (16)$$

which is positive definite and radially unbounded for  $e_\theta \in [-\pi, \pi]$ , and whose time derivative is

$$\dot{V} = e_x \dot{e}_x + e_y \dot{e}_y + \sin(e_\theta) \dot{e}_\theta = e_x (v \cos(\theta) - v_d \cos(\theta_d)) + e_y (v \sin(\theta) - v_d \sin(\theta_d)) + \sin(e_\theta) (\omega - \omega_d). \quad (17)$$



By considering the auxiliary inputs  $\delta v$  and  $\delta\omega$  in a backstepping fashion, we have

$$v = v_d + \delta v, \quad \omega = \omega_d + \delta\omega, \quad (18)$$

and, by simple trigonometric manipulations and after substitution of the dynamics of the error (14) along the system dynamics (7), leads to

$$\begin{aligned} \dot{V} = & -2v_d e_x \sin\left(\frac{e_\theta}{2}\right) \sin\left(\frac{\delta}{2}\right) + 2v_d e_y \sin\left(\frac{e_\theta}{2}\right) \cos\left(\frac{\delta}{2}\right) + \\ & + \delta v (e_x \cos(\theta) + e_y \sin(\theta)) + \sin(e_\theta) \delta\omega, \end{aligned}$$

with  $\delta$  being defined as  $\delta = \theta + \theta_d$ . Using (15) and after some algebra, we have,

$$\begin{aligned} \dot{V} = & 2v_d e_{xy} \sin\left(\frac{e_\theta}{2}\right) \sin\left(\psi - \frac{\delta}{2}\right) + \sin(e_\theta) \delta\omega + \\ & + \delta v e_{xy} \cos(\psi - \theta), \end{aligned} \quad (19)$$

and hence, by setting the auxiliary inputs

$$\begin{aligned} \delta v = & -k_p e_{xy} \cos(\psi - \theta), \\ \delta\omega = & \frac{1}{\sin(e_\theta)} \left( -2v_d e_{xy} \sin\left(\frac{e_\theta}{2}\right) \sin\left(\psi - \frac{\delta}{2}\right) \right) - k_\theta \sin(e_\theta) \\ = & -v_d e_{xy} \frac{1}{\cos\left(\frac{e_\theta}{2}\right)} \sin\left(\psi - \frac{\delta}{2}\right) - k_\theta \sin(e_\theta), \end{aligned} \quad (20)$$

with  $k_p > 0$  and  $k_\theta > 0$  design parameters, we have

$$\dot{V} = -k_p e_{xy}^2 \cos^2(\theta - \psi) - k_\theta \sin^2(e_\theta), \quad (21)$$

which is negative semi-definite. More precisely,

$$\dot{V} = 0 \text{ when } \begin{cases} e_{xy} = 0 \text{ and } e_\theta = 0, \\ e_\theta = 0 \text{ and } \theta = \psi \pm \frac{\pi}{2}. \end{cases}$$

The first case is the desired equilibrium. In the second case, by applying (20), we have  $\delta v = 0$  and

$$\delta\omega = -v_d e_{xy} \sin\left(\psi - \frac{\delta}{2}\right) = -v_d e_{xy} \sin\left(\frac{e_\theta}{2} \pm \frac{\pi}{2}\right) = \pm v_d e_{xy},$$

which is an equilibrium point only if  $e_{xy} = 0$ . This proves global asymptotic stability by Lasalle theorem.

### B. Lyapunov Based Control of the tracked vehicle

Let us consider the dynamics (9) with the inputs that contain the lateral slippage  $\alpha$ , i.e.

$$v = (v_d + \delta v) \cos(\alpha), \quad \omega = \omega_d + \delta\omega. \quad (22)$$

We also modify the Lyapunov function (16) as follows:

$$V = \frac{1}{2} (e_x^2 + e_y^2) + (1 - \cos(e_\theta + \alpha_d)) \quad (23)$$

where  $\alpha_d = f\left(\frac{v_d}{\omega_d}\right)$ , with  $f(\cdot)$  that could be defined as in (11). This function is positive definite and has an equilibrium point in  $e_{xy} = 0$  and  $e_\theta = -\alpha_d$ , hence having a tracking reference for  $\theta$  in  $\theta_d - \alpha_d$  and giving up the possibility to track  $\theta_d$ . This is somewhat expected from the dynamics (9): the effect of  $\alpha$  is to make impossible to simultaneously track  $x_d$ ,  $y_d$  and  $\theta_d$ . Indeed, if  $\theta_d = \theta$ , it

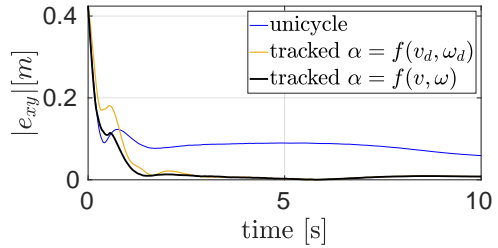


Fig. 5. Cartesian tracking error for a spiral-like trajectory. The blue line is the reference unicycle controller, the yellow and black lines are the slippage-aware controller with and without the approximation  $\alpha \approx \alpha_d = f(v_d, \omega_d)$ .

is impossible to generate a velocity that keeps  $x$  and  $y$  on  $x_d$  and  $y_d$ , which are generated by a unicycle-like dynamics (hence, with  $\alpha = 0$ ). However, from a practical point of view, it is not an issue to track  $\theta_d - \alpha_d$  instead of  $\theta_d$ , since an appropriate reference for  $\theta_d + \alpha_d$  could be designed at the planning level, based on desired values of  $v_d$  and  $\omega_d$  and (11). By choosing the two control values as per Equation (22), following the same rationale of Section IV-A, we find that the derivative of the Lyapunov function (23), obtained after some basic trigonometric simplifications, is given by:

$$\begin{aligned} \dot{V} = & e_x \dot{e}_x + e_y \dot{e}_y + \sin(e_\theta + \alpha_d) (\dot{e}_\theta + \dot{\alpha}_d) \\ = & 2v_d e_{xy} \sin\left(\frac{\alpha + e_\theta}{2}\right) \sin\left(\psi - \frac{\alpha + \delta}{2}\right) + \\ & + \delta v e_{xy} \cos(\psi - (\alpha + \theta)) + \sin(e_\theta + \alpha_d) (\delta\omega + \dot{\alpha}_d), \end{aligned} \quad (24)$$

where we set  $\delta = \theta + \theta_d$ . If we choose the new auxiliary controllers as

$$\begin{aligned} \delta v = & -k_p e_{xy} \cos(\psi - (\theta + \alpha)), \\ \delta\omega = & -v_d e_{xy} \frac{1}{\cos\left(\frac{\alpha + e_\theta}{2}\right)} \sin\left(\psi - \frac{\alpha + \delta}{2}\right) - k_\theta \sin(e_\theta + \alpha_d) - \dot{\alpha}_d, \end{aligned} \quad (25)$$

we finally have

$$\dot{V} = -k_p e_{xy}^2 \cos^2(\psi - (\alpha + \theta)) - k_\theta \sin^2(e_\theta + \alpha_d). \quad (26)$$

which is negative semidefinite. Using Lasalle arguments, we can prove convergence to the equilibrium  $e_{xy} = 0$  and  $e_\theta = -\alpha_d$ . It is worth observing that (25) is actually implicit since  $\delta v$  and  $\delta\omega$  are actually present in the expression of  $\alpha$  (that depends on  $R$  (11), which on its turn depends on  $v$  and  $\omega$ , function of  $\delta v$ ,  $\delta\omega$ ). An initial guess for the solution can be found by setting  $\alpha \approx \alpha_d$  then iteratively solve the system (25) till convergence. To show the global stability of the system we performed a simulation (see Fig. 5) with the designed controllers applied to the kinematic model (9). The aim is to track a spiral-like reference trajectory of increasing radius of curvature (i.e.,  $\dot{\alpha}_d$  is not null) starting with an initial state  $[x_0, y_0, \theta_0] = [0.3, 0.3, 0.2]$ . The figure shows that the impact on performances of considering the approximation  $\alpha \approx \alpha_d$  is minimal.

## V. EXPERIMENTAL RESULTS

We report here the simulation results comparing the performances of the reference unicycle controller (20), with the proposed slippage-aware control law (25). Both control laws are mapped into wheels speeds by inverting (8). In the case of the slippage-aware controller we also apply a *feed-forward* compensation of the longitudinal slippages  $\beta_{L/R}(\omega_L, \omega_R)/r$ , estimated with the regressor of Section III-b. Differently from the simulation in the previous section, where we used model (9), in this simulation we

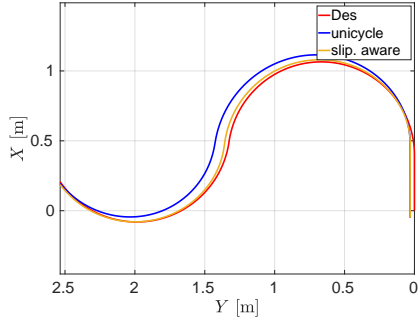


Fig. 6. Trajectory plot for the closed loop control of the chicane reference trajectory (red line). Both the unicycle controller (blue line) and the proposed slippage-aware controller (yellow line) are reported.

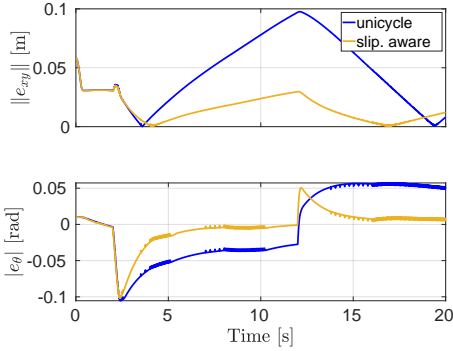


Fig. 7. Tracking errors for the closed loop control of the chicane reference trajectory in Figure 6. (upper plot) Cartesian error, (bottom plot) orientation error. (blue) unicycle controller, (yellow) slippage-aware controller.

implement the dynamics of the distributed parameter model (5). The simulation is part of the Locosim framework [20]<sup>1</sup>. As terrain model, we assume a firm ground (i.e., cohesion is null) with a friction coefficient  $\mu = 0.1$ . As reference trajectory we created a chicane (see Fig. 6) with a deliberately discontinuous velocity profile in  $v_d$  and  $\omega_d$ . The robot is meant to accelerate forward in a linear motion then a left turn is followed by a right turn. The velocity reference is as follows

$$v_d = \begin{cases} v_{max}(t - t_1) & 0 \leq t \leq t_1, \\ v_{max} & t_1 \leq t \leq t_{end}, \end{cases}, \omega_d = \begin{cases} 0 & 0 \leq t \leq t_1, \\ \omega_{max} & t_1 \leq t \leq t_2, \\ -\omega_{max} & t_2 \leq t \leq t_{end}, \end{cases}$$

with  $t_1 = 2$  s,  $t_2 = 12$  s and  $t_{end} = 20$  s,  $v_{max} = 0.2$  m/s and  $\omega_{max} = 0.3$  rad/s. The reference states are obtained by integration of (7), while the initial state is  $[x_0, y_0, \theta_0] = [0.05m, 0.03m, 0.01rad]$ . In the simulation, we simulate the presence of actuation uncertainties by adding a Gaussian noise  $n \sim \mathcal{N}(0, 0.02)$  to the actuator inputs. Figure 6 reports the  $X - Y$  plots for the simulation experiments. Figure 7, instead, shows that the unicycle controller has a maximum Cartesian error of 10 cm, the slippage-aware controller manages to keep it always below 3 cm. The tracking of the orientation is also significantly improved with the slippage-aware controller. In Figure 8 we report a comparison of the tracking performances of the slippage-aware controller both in simulation and real experiments for the same chicane trajectory. Experimental results are also reported in the accompanying video<sup>2</sup>. Figure 9 shows the results of the prediction of  $\beta_L$  (upper plot),  $\beta_R$  (middle) and  $\alpha$  (bottom). The prediction for  $\beta_L$  and  $\beta_R$  is accurate

<sup>1</sup>Source code is available at the following link.

<sup>2</sup>The accompanying video can be found at this link

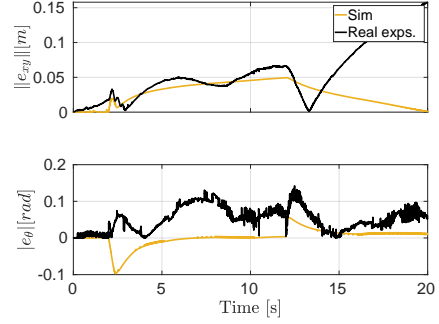


Fig. 8. Comparison of tracking errors for the slippage-aware controller in simulation (yellow) and real experiments (black). The reference trajectory is in red. (upper plot) Cartesian error, (bottom plot) orientation error.

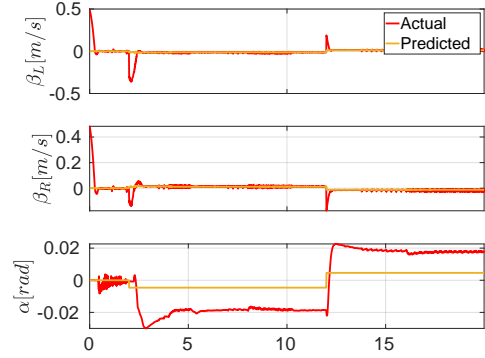


Fig. 9. Longitudinal slippage for (upper plot) left track (middle plot) right track and (bottom plot) lateral slippage. The red plot is the actual value while the yellow plot is the value, used in the slippage-aware controller, predicted with (11).

in steady state, while it exhibits an error when acceleration takes place, thus showing a further complex dependency on accelerations. Albeit the sign is correct (i.e., opposite to the steering speed  $\omega$ ), the prediction of  $\alpha$ , which is based on the desired values  $v_d$  and  $\omega_d$ , is inaccurate and shows a constant under-compensation. Interestingly, we can highlight that at  $t = t_1 = 2$  s (discontinuity from linear to angular motion) there is a delay of the actual  $\alpha$  w.r.t the predicted  $\alpha_d$ : this is in agreement with a physical phenomena [21] (well captured by the dynamic model) for which, when the vehicle is about to start turning, there is a progressive build-up of the steering forces, while the vehicle still goes on a straight path, until they reach a critical value for the steering maneuver. This effect cannot be captured by a model which is purely kinematic.

## VI. CONCLUSIONS

We have focused on the problem of trajectory control for tracked vehicles. Our approach is based on the use of a pseudo-kinematic model, which encapsulates in a small number of parameters the most relevant dynamic effects of this type of vehicles. The model captures both linear and lateral slippage effects. We have found effective ways to estimate these parameters as a function of the track velocities. This result underpinned the development of a nonlinear control strategy, which featured a high level of tracking performance even in the most critical conditions (i.e., vehicle moving at high speed or on a slippery terrain).

The application of our strategy allowed us to approximate a unicycle kinematics for the closed-loop vehicle. This feature discloses important future opportunities to integrate our control strategy with very efficient motion planning solutions, which is one of our obvious future research directions. In addition, we plan to adapt our control strategy to sloped and uneven terrains. Finally, a

remarkable research effort is the study of estimation algorithms for the terrain parameters.

[21] H. E. Merritt, "The Evolution of a Tank Transmission," *Proceedings of the Institution of Mechanical Engineers*, vol. 154, no. 1, pp. 412–428, 1946.

## REFERENCES

- [1] Z. Shiller, W. Serate, and M. Hua, "Trajectory planning of tracked vehicles," *Proceedings - IEEE International Conference on Robotics and Automation*, vol. 3, no. June 1993, pp. 796–801, 1993.
- [2] S. Laughery, G. Gerhart, and P. Muench, "Evaluating Vehicle Mobility Using Bekker's Equations," *US Army TARDEC*, p. 10, 2000.
- [3] J. Y. Wong, *Theory of ground vehicles*. John Wiley & Sons, 2022.
- [4] M. Ahmadi, V. Polotski, and R. Hurteau, "Path tracking control of tracked vehicles," *Proceedings-IEEE International Conference on Robotics and Automation*, vol. 3, no. April, pp. 2938–2943, 2000.
- [5] A. T. Le, D. C. Rye, and H. F. Durrant-Whyte, "Estimation of track-soil interactions for autonomous tracked vehicles," *Proceedings - IEEE International Conference on Robotics and Automation*, vol. 2, no. April 1997, pp. 1388–1393, 1997.
- [6] X. Zhao, E. Lu, Z. Tang, C. Luo, L. Xu, and H. Wang, "Trajectory prediction method for agricultural tracked robots based on slip parameter estimation," *Computers and Electronics in Agriculture*, vol. 222, no. December 2023, 2024.
- [7] Z. Song, S. Hutangkabodee, Y. H. Zweiri, L. D. Seneviratne, and K. Althoefer, "Identification of soil parameters for unmanned ground vehicles track-terrain interaction dynamics," *Proceedings of the SICE Annual Conference*, pp. 1651–1656, 2004.
- [8] S. A. A. Moosavian and A. Kalantari, "Experimental slip estimation for exact kinematics modeling and control of a Tracked Mobile Robot," *2008 IEEE/RSJ International Conference on Intelligent Robots and Systems, IROS*, pp. 95–100, 2008.
- [9] M. Piccinini, S. Taddei, M. Larcher, M. Piazza, and F. Biral, "A Physics-Driven Artificial Agent for Online Time-Optimal Vehicle Motion Planning and Control," *IEEE Access*, vol. 11, pp. 46 344–46 372, 2023.
- [10] Y. Kanayama, Y. Kimura, F. Miyazaki, and T. Noguchi, "A stable tracking control method for an autonomous mobile robot," in *Proceedings., IEEE International Conference on Robotics and Automation*, 1990, pp. 384–389 vol.1.
- [11] L. Caracciolo, A. de Luca, and S. Iannitti, "Trajectory tracking control of a four-wheel differentially driven mobile robot," in *Proceedings 1999 IEEE International Conference on Robotics and Automation (Cat. No.99CH36288C)*, vol. 4, 1999, pp. 2632–2638 vol.4.
- [12] T. Zou, J. Angeles, and F. Hassani, "Dynamic modeling and trajectory tracking control of unmanned tracked vehicles," *Robotics and Autonomous Systems*, vol. 110, pp. 102–111, 2018. [Online]. Available: <https://doi.org/10.1016/j.robot.2018.09.008>
- [13] N. Strawa, D. I. Ignatyev, A. C. Zolotas, and A. Tsourdos, "Online learning and updating unmanned tracked vehicle dynamics," *Electronics (Switzerland)*, vol. 10, no. 2, pp. 1–38, 2021.
- [14] A. D. Sabiha, M. A. Kamel, E. Said, and W. M. Hussein, "ROS-based trajectory tracking control for autonomous tracked vehicle using optimized backstepping and sliding mode control," *Robotics and Autonomous Systems*, vol. 152, p. 104058, 2022. [Online]. Available: <https://doi.org/10.1016/j.robot.2022.104058>
- [15] J. L. Martínez, A. Mandow, J. Morales, S. Pedraza, and A. García-Cerezo, "Approximating kinematics for tracked mobile robots," *International Journal of Robotics Research*, vol. 24, no. 10, pp. 867–878, 2005.
- [16] J. P. Laumond, S. Sekhavat, and F. Lamiraux, *Guidelines in nonholonomic motion planning for mobile robots*. Berlin, Heidelberg: Springer Berlin Heidelberg, 1998, pp. 1–53. [Online]. Available: <https://doi.org/10.1007/BFb0036070>
- [17] M. K. Kar, "Prediction of track forces in skid-steering of military tracked vehicles," *Journal of Terramechanics*, vol. 24, no. 1, pp. 75–84, 1987.
- [18] S. Al-Milli, L. D. Seneviratne, and K. Althoefer, "Track-terrain modelling and traversability prediction for tracked vehicles on soft terrain," *Journal of Terramechanics*, vol. 47, no. 3, pp. 151–160, 2010. [Online]. Available: <http://dx.doi.org/10.1016/j.jterra.2010.02.001>
- [19] Robo-dyne, "MEGA MAXXII: Unmanned Tracked Ground Vehicle," Accessed on 09/2024. [Online]. Available: <https://www.robo-dyne.com/mega-maxxii-ugv-tracked-robot-vehicle/>
- [20] M. Focchi, F. Roscia, and C. Semini, "Locosim: an open-source cross-platform robotics framework," in *Synergetic Cooperation between Robots and Humans. CLAWAR 2023. Lecture Notes in Networks and Systems*, 2024, pp. 395–406.